Location Optimization of Monopole Equivalent Sources in Wave Superposition Method

Shaowei Wu

School of Energy and Power Engineering, Wuhan University of Technology, Wuhan, 430063, P. R. China.
The Second Ship Design Institute of Wuhan, Wuhan, 430063, P. R. China.

Yang Xiang

School of Energy and Power Engineering, Wuhan University of Technology, Wuhan, 430063, P. R. China.

(Received 10 December 2017; accepted 5 February 2018)

In wave superposition method, the prediction accuracy of acoustic pressure heavily depends on the locations of equivalent sources. In this paper, the prediction accuracy corresponding to monopole equivalent source is studied. According to analysis in this paper, when the velocities on some boundary nodes are inversely calculated using the predicted pressures, there is velocity reconstruction error, and the prediction error of the acoustic pressure and the velocity reconstruction error are closely related. The relationship between them is theoretically derived and indicates that the prediction error decreases with a decrease in velocity reconstruction error. Based on these findings, a method to determine the optimal locations by minimizing the normalized velocity reconstruction error is proposed. A frequency threshold criterion is devised to give the frequency range for certain number of equivalent sources within which good prediction accuracy of the acoustic pressure can be obtained. The proposed method is validated by simulation and experiment, respectively. The results show that the method significantly reduces prediction errors and is feasible.

1. INTRODUCTION

Boundary element method (BEM) is established as a well-known numerical tool for predicting acoustic pressure in infinite domain. In the BEM, boundary surface discretization is only required, and the Sommerfeld radiation condition at infinity is naturally satisfied.[1–3] However, the system matrices of BEM are usually non-sparse and non-symmetric, which increases the processing time and storage requirements.[2] Furthermore, the non-uniqueness problem occurs at characteristic wave numbers corresponding to interior problems.[2,3] Different methods including the CHIEF and the Burton-Miller methods to overcome the non-uniqueness problem have been devised.[1–4] In the CHIEF method, the integral formulation is modified by adding equations to enforce solutions to vanish at points in the interior. Thus, the fictitious solutions can be differentiated from the true ones. But there is a lack of rigorous criteria for selecting interior points and determining the limit of stability.[3] The Burton-Miller method, in which the integral equation is combined with its normal derivative, theoretically precludes non-unique solutions. However, the various orders of singular integrals of Green's function must be numerically described and can lead to inefficiencies in computation.[4] During the past few decades, tremendous progresses in the development of BEM are moving the application of BEM in predicting acoustic radiation in infinite domain. For example, with the recent developments in fast multipole BEM, the computational efficiency is significantly improved.[5] The relevant work of BEM is still on its way.[6–9]

Koopmann et al. proposed the wave superposition method (WSM) based on the idea that the radiated acoustic field of a radiator can be constructed as a superposition of the fields generated by an array of equivalent sources located on an auxiliary surface in the radiator.[10] The source strengths are determined by the specific normal velocity distribution on boundary surface. Thus, the singular integrals of Green's function,[4,11–14] which are involved in BEM when the acoustic pressure prediction points are located on the boundary surface, are eliminated. Only matrix operations are needed for the acoustic pressure prediction. Therefore, this method greatly simplifies the process of acoustic pressure prediction and is easily realized using computer programming. WSM has been applied to calculation of acoustic radiation.[15–17] However, the prediction accuracy of acoustic pressure using this method strongly depends on the locations of the equivalent sources, particularly for the radiators with complex geometric shapes. Determining the locations becomes a problem. If the sources are far from the boundary surface, the system equations become ill-conditioned and the prediction accuracy of acoustic pressure is greatly affected. Alternatively, if equivalent sources are located near the boundary surface, the singularity occurs and erroneous predicted results will be obtained. The equivalent source locations are distinguishing for different structures. These lead to that until now there is no available commercial software of WSM to predict acoustic pressure.

To determine the equivalent source locations, some researches have been proceeded. Bai provided an effective methodology for finding the optimal distance for WSM ap-

plications, and indicated that the optimal distance was not a unique value and may well depend on many factors.[18] Fahnline studied the prediction accuracy and stability of the wave superposition method using singular-value decomposition, and provided physical insight into the nature of an acoustic field by the approximate singular-function expansion of the acoustic radiation.[19] His research further showed that the nodes should be equally spaced. The cause of the non-uniqueness problem (due to too small singular value) was also discussed. Hwang and Chang developed a regular integral equation for the exterior acoustic radiation based on the surface source distribution.[20] It has been indicated that the offset distance between the equivalent source and boundary surface must be larger than one-quarter of element size for a certain meshing pattern. Gounot and Musafir devised a genetic algorithm to search for the optimal equivalent source sets.[21–23] This approach permits a good reconstitution of the pressure field by using very few monopoles. However, this search algorithm fails for large number of sources. Zellers and Wu analyzed the diagonal terms in related matrices.[24–27] The diagonal terms were substituted by the derived approximate analytical expression self-terms. As an example of the application of the technique, acoustic radiation from a uniformly pulsating sphere was analyzed and compared with the analytic solution. The results showed that the approximate analytical expressions of the monopoles were only consistent with the analytical solutions in the low-frequency range.

In this paper, the relationship between the prediction error of the acoustic pressure and velocity reconstruction error on the boundary is theoretically derived. An optimization method to determine the locations of equivalent sources is proposed to improve the prediction accuracy. A frequency threshold criterion is devised to make the predicted pressure accuracy acceptable. The applicability of this proposed method is demonstrated by numerically investigating the acoustic field of two models including a uniformly pulsating sphere and designed shell structure. The proposed method is further validated by experiments of a cylindrical shell and a clamped plate.

2. THEORETICAL BACKGROUND

The wave superposition method (WSM) is based on the idea that the radiated acoustic field of a radiator can be constructed as a superposition of the fields generated by an array of simple sources, which are called equivalent sources and located on an auxiliary surface enclosed in the radiator. The resulting pressure at a receiver point r is defined as[10]:

$$p(\mathbf{r}) = \mathrm{i}\rho\omega \int_V q(\mathbf{r}_0) g(|\mathbf{r}-\mathbf{r}_0|) \mathrm{d}V(\mathbf{r}_0); \tag{1}$$

where $\mathrm{i}^2 = -1$; ρ is the mean density of the medium; ω is the angular frequency of the harmonic vibration of surface S, which encloses volume V of the radiator; $q(\mathbf{r}_0)$ is the strength of the simple source distribution,[10] which is evaluated at $\mathbf{r}_0$ inside V, as shown in Fig. 1a; and $g(|\mathbf{r}-\mathbf{r}_0|) = -e^{\mathrm{i}k|\mathbf{r}-\mathbf{r}_0|}/4\pi|\mathbf{r}-\mathbf{r}_0|$ is the free-space Green's function,

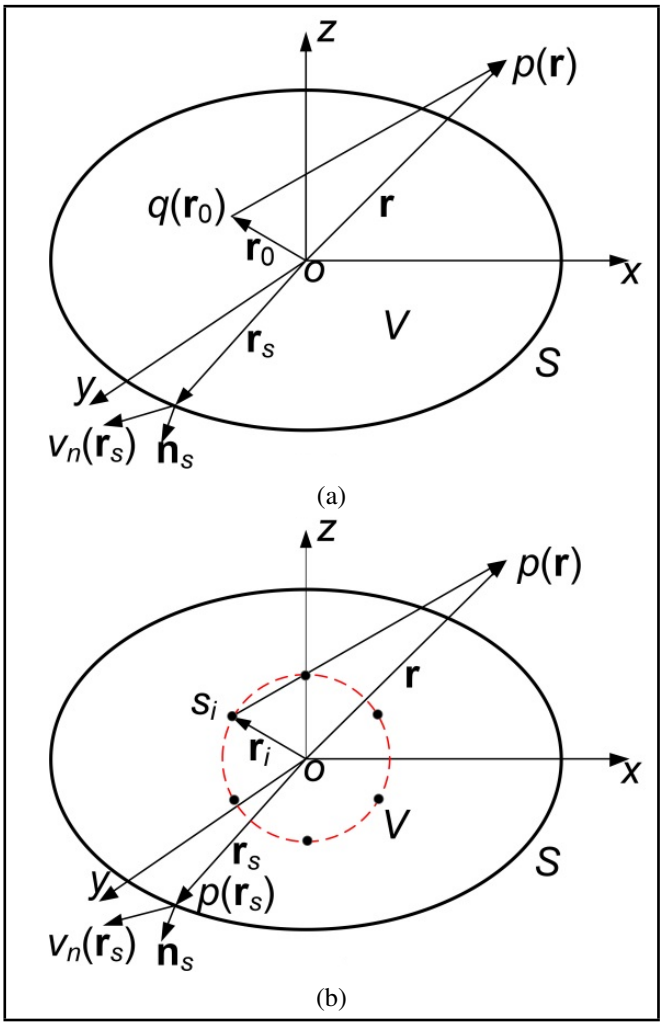

Figure 1. Diagram of the wave superposition method and equivalent source array.

where $k = \omega/c$ is acoustic wavenumber, and c is the speed of acoustic in the acoustic medium.

There is no restriction on the location of $\mathbf{r}_0$, and it can be placed anywhere in V. In general, 0these simple sources are assumed to distribute over on surface of a fictitious spherical shell. Through some algebraic operations and discretization, Equation (1) is rewritten as[10]:

$$\hat{p}(\mathbf{r}) = \sum_{i=1}^{N} s_i g(\mathbf{r}, \mathbf{r}_i); \tag{2}$$

where $\hat{p}(\mathbf{r})$ denotes an approximation of $p(\mathbf{r})$; $\mathbf{r}_i$ is the location of the ith equivalent source on the auxiliary surface, as shown in Fig. 1b; and s_i is the source strength of the ith equivalent source.

The boundary condition on the surface of the radiator is defined by:

$$\nabla p(\mathbf{r}_s) \cdot \mathbf{n}_s = -\mathrm{i}k\rho c v(\mathbf{r}_s) \quad \text{on } S; \tag{3}$$

where ∇ represents the gradient operator with respect to the receiver location $\mathbf{r}_s$ on the boundary surface; $\mathbf{n}_s$ is the unit normal vector at location $\mathbf{r}_s$ on the boundary surface; and $v(\mathbf{r}_s)$ is the normal velocity at $\mathbf{r}_s$. Substituting Eq. (2) into Eq. (3) and applying it to N nodes on the surface of the radiator, the

source strengths can be determined. Thus, the radiated acoustic pressure at any field point is determined as:

$$\hat{p}(\mathbf{r}) = \sum_{j=1}^{N} \left(\sum_{i=1}^{N} g(\mathbf{r}, \mathbf{r}_i) \mathbf{D}_{ij}^{-1} \right) v(\mathbf{r}_{sj}); \quad (4)$$

where $v(\mathbf{r}_{sj})$ is the normal velocity corresponding to the jth node on the boundary; and:

$$\mathbf{D}_{ij} = \frac{1}{\mathrm{i}k\rho c} \frac{\partial g(\mathbf{r}_{si}, \mathbf{r}_j)}{\partial \mathbf{n}_{si}}. \quad (5)$$

3. EQUIVALENT SOURCE LOCATION OPTIMIZATION

3.1. Velocity Reconstruction Error

Equation (3) indicates that the pressure and the vibration velocity on the boundary are not independent. In this section, the relationship between the prediction error of acoustic pressure and the surface velocity reconstruction error is analyzed. From Eqs. (3) and (4), the normal velocity at arbitrary location $\mathbf{r}_s$ on the boundary can be expressed as:

$$\hat{v}(\mathbf{r}_s) = \sum_{j=1}^{N} \left(\frac{1}{\mathrm{i}k\rho c} \sum_{i=1}^{N} \frac{\partial g(\mathbf{r}_s, \mathbf{r}_i)}{\partial \mathbf{n}_s} \mathbf{D}_{ij}^{-1} \right) v(\mathbf{r}_{sj}) = \sum_{j=1}^{N} N_j(\mathbf{r}_s) v(\mathbf{r}_{sj}); \quad (6)$$

where $N_j(\mathbf{r}_s)$ is the velocity interpolation function. When $\mathbf{r}_s = \mathbf{r}_{sh}$ ($\mathbf{r}_{sh}$ is the location of the hth node on the boundary surface), $N_j(\mathbf{r}_{sh})$ is written as:

$$N_j(\mathbf{r}_{sh}) = \frac{1}{\mathrm{i}k\rho c} \sum_{i=1}^{N} \frac{\partial g(\mathbf{r}_{sh}, \mathbf{r}_i)}{\partial \mathbf{n}_{sh}} \mathbf{D}_{ij}^{-1} = \sum_{i=1}^{N} \mathbf{D}_{hi} \mathbf{D}_{ij}^{-1}. \quad (7)$$

Equation (7) indicates that $N_j(\mathbf{r}_{sh})$ is the summation of the product of the hth row of matrix $\mathbf{D}$ and the jth column of $\mathbf{D}^{-1}$. Thus, $N_j(\mathbf{r}_{sh})$ is exactly unity when $h = j$ and zero when $h \neq j$ due to $\mathbf{D}\mathbf{D}^{-1} = \mathbf{E}$, where $\mathbf{E}$ is the identity matrix. Therefore, $N_j(\mathbf{r}_{sh}) = \delta_{hj}$, where δ_{hj} is the Kronecker delta. Because of the property of the Kronecker delta, the calculated surface normal velocities on the nodes are identical to the prescribed values, which are used to obtain the source strengths, i.e., $\hat{v}(\mathbf{r}_{sh}) = v(\mathbf{r}_{sh}),\ h = 1, 2, \cdots, N$. Because the prescribed normal velocities on these surface nodes can be exactly reconstructed and the imaginary part of $N_j(\mathbf{r}_{sj})$ is zero at these nodes, the imaginary part of $N_j(\mathbf{r}_s)$ vanishes when N approaches infinity. However, it is not always zero for finite N values. This behavior results in velocity reconstruction errors on the surface, i.e., the reconstructed velocity $\hat{v}(\mathbf{r}_s)$ is not identical to the prescribed value $v(\mathbf{r}_s)$ when $\mathbf{r}_s \neq \mathbf{r}_{sh}$.

In this paper, the errors of the predicted acoustic pressure and the reconstructed velocity on the boundary surface are represented by $\varepsilon_p = p(\mathbf{r}_s) - \hat{p}(\mathbf{r}_s)$ and $\varepsilon_v = \mathbf{v}(\mathbf{r}_s) - \hat{\mathbf{v}}(\mathbf{r}_s)$, respectively, where $\mathbf{v}(\mathbf{r}_s) \cdot \mathbf{n}_s = v(\mathbf{r}_s)$ and $\hat{\mathbf{v}}(\mathbf{r}_s) \cdot \mathbf{n}_s = \hat{v}(\mathbf{r}_s)$. Because $\hat{p}(\mathbf{r}_s)$ and $\hat{\mathbf{v}}(\mathbf{r}_s)$ satisfy Eq. (3), the following equation is obtained.

$$\mathrm{i}k\rho c\varepsilon_v(\mathbf{r}_s) = \nabla \varepsilon_p(\mathbf{r}_s). \quad (8)$$

The linearized equations of the conservation of mass and state are given as[28]:

$$\frac{\partial \rho'(\mathbf{r}_s, t)}{\partial t} + \rho \nabla \cdot v(\mathbf{r}_s, t) = 0, p(\mathbf{r}_s, t) \approx c^2 \rho'(\mathbf{r}_s, t); \quad (9)$$

where $\rho'(\mathbf{r}_s, t)$ is the fluctuating quantity of the medium density. Only considering harmonic steady state conditions, the pressure $p(\mathbf{r}_s, t)$ and vibration velocity $v(\mathbf{r}_s, t)$ can be written as $p_t(\mathbf{r}_s, t) = p(\mathbf{r}_s)e^{-\mathrm{i}\omega t}$ and $v_t(\mathbf{r}_s, t) = v(\mathbf{r}_s)e^{-\mathrm{i}\omega t}$. Their approximations are given as $\hat{p}_t(\mathbf{r}_s, t) = \hat{p}(\mathbf{r}_s)e^{-\mathrm{i}\omega t}$ and $\hat{v}_t(\mathbf{r}_s, t) = \hat{v}(\mathbf{r}_s)e^{-\mathrm{i}\omega t}$. Thus, the following equation is obtained.

$$\nabla \cdot \varepsilon_v(\mathbf{r}_s) = \frac{\mathrm{i}k}{\rho c} \varepsilon_p(\mathbf{r}_s). \quad (10)$$

Substituting Eq. (8) into Eq. (10) yields:

$$\nabla^2 \varepsilon_p(\mathbf{r}_s) + k^2 \varepsilon_p(\mathbf{r}_s) = 0. \quad (11)$$

It can be noted that $\varepsilon_p(\mathbf{r}_s)$ satisfies the Helmholtz equation. Equation (8) can be rewritten as:

$$\mathrm{i}k\rho c\varepsilon_v(\mathbf{r}_s) \cdot \mathbf{n}_s = \frac{\partial \varepsilon_p(\mathbf{r}_s)}{\partial \mathbf{n}_s}. \quad (12)$$

Thus, this boundary condition is satisfied by $\varepsilon_p(\mathbf{r}_s)$. Because both $p(\mathbf{r})$ and $\hat{p}(\mathbf{r})$ satisfy the Sommerfeld radiation condition, the following equation at infinity is obtained.

$$\lim_{r \to \infty} r^{\alpha} \left(\frac{\partial \varepsilon_p(\mathbf{r})}{\partial r} + \mathrm{i}k\varepsilon_p(\mathbf{r}) \right) = 0; \quad (13)$$

where r denotes a cylindrical or spherical polar radius, and α is equal to $1/2$ in the two-dimensional case (2D) and equal to 1 in three-dimensional case (3D). Hence, $\varepsilon_p(\mathbf{r}_s)$ satisfies the Sommerfeld radiation condition at infinity.

Analogous to the pressure wave, an error wave of the pressure prediction that corresponds to the velocity reconstruction error appears to be radiated from the radiator. Obviously, $\varepsilon_p(\mathbf{r}_s)$ is small when $\varepsilon_v(\mathbf{r}_s)$ is small. Thus, $\varepsilon_v(\mathbf{r}_s)$ can be used to reflect the prediction accuracy of the acoustic pressure. As a result, the optimal locations can be determined by minimizing the velocity reconstruction error. In WSM, the non-uniqueness problems of monopole equivalent source at the eigen-frequencies that correspond to the locations of the sources can be eliminated by adjusting the locations. Therefore, the non-uniqueness problems can be avoided in the optimal locations.

3.2. Equivalent Source Location Determination

To accurately predict the acoustic pressure, the dipole matrix $\mathbf{D}$ should be diagonally dominant. This condition requires that each source must be paired with the corresponding node on the boundary surface, and that the distance between the source

and node is less than that from any other source to the node. However, only a few structures, such as the sphere and infinite circular cylinder, can satisfy this condition. To reduce the optimization parameters for determining the optimal locations, equivalent sources are located on an auxiliary surface that is retracted from the actual structure boundary by scale coefficient $S_c (0 < S_c < 1)$. The auxiliary surface has a similar geometric shape to the radiator. The coordinates of the sources are obtained by multiplying Sc with the surface nodes. Thus, the parameters are reduced to one.

To determine the optimal S_c, a method is proposed by minimizing the normalized velocity reconstruction error, which is defined as:

$$\varepsilon_v = \frac{\int\limits_S |v(\mathbf{r}_s) - \hat{v}(\mathbf{r}_s)| \mathrm{d}S}{\int\limits_S |v(\mathbf{r}_s)| \mathrm{d}S} \times 100\% \approx \frac{\sum\limits_{j=1}^{N} S_j \left|v(\mathbf{r}_{sj}) - \hat{v}(\mathbf{r}_{sj})\right|}{\sum\limits_{j=1}^{N} S_j \left|v(\mathbf{r}_{sj})\right|} \times 100\%. \quad (14)$$

To calculate ε_v, the boundary surface is divided into with two meshing patterns: modes A and B. In Eq. (14), S_j is the area of the jth node in mode B. Here, it should be noted that the nodes of mode A do not coincide with those of mode B. The nodes of mode A are used to obtain equivalent sources, and the prescribed velocities on the nodes are used to calculate the acoustic pressure. According to Eq. (6), the constructed velocities $\hat{v}(\mathbf{r}_{sj})$ on the nodes of mode B are interpolated using the sjprescribed velocities on the nodes of mode A for each S_c. For each S_c, ε_v is obtained by substituting $\hat{v}(\mathbf{r}_{sj})$ and the prescribed velocities $v(\mathbf{r}_{sj})$ on the nodes of mode B into Eq. (14). Then S_c that corresponds to the minimum ε_v is selected as the optimal value. The radiated acoustic vpressure is predicted in the determined auxiliary surface. The designed objective function is:

$$\begin{cases} \text{Objective function} = \min(\varepsilon_v(Sc, k)) \\ Sc \in (0,1), k = k_1, k_2, \cdots, k_n \end{cases}. \quad (15)$$

3.3. Frequency Threshold Criterion

It is known that the acoustic wavelength decreases with the increase in vibration frequency. Therefore, for a certain number of equivalent sources, the threshold of frequency within which the prediction accuracy of acoustic pressure in WSM is acceptable is limited. Besides that, the threshold is distinguishing when the equivalent sources are located on different auxiliary surfaces. Hence, it is indispensable to give the threshold in the optimal auxiliary surface to ensure the predicted results are acceptable for the given number of equivalent sources.

When the sources are located on the determined auxiliary surface, the radiated acoustic pressure in the exterior region to radiator can be expressed as[10]:

$$p(\mathbf{r}) = \mathrm{i}\rho\omega\delta_\tau \int\limits_\sigma q(\mathbf{r}_\sigma) g(\mathbf{r}, \mathbf{r}_\sigma) \mathrm{d}\sigma(\mathbf{r}_\sigma); \quad (16)$$

where σ is the determined auxiliary surface and δ_τ is a constant value for thickness.[10] The discretization of Eq. (16) can be achieved by subdividing the auxiliary surface into a set of small quadrilateral or triangular elements. The integral over the auxiliary surface is approximated by summations of integrals over each element. The spatial coordinates and acoustic variables within an element can be related to the nodal values by shape functions. Then, the appropriately weighted Gaussian quadrature formula is used to calculate the element integrals. Using the isoparametric surface element, the global coordinate $\mathbf{r}_\sigma$ and the source strength $q(\mathbf{r}_\sigma)$ on each element can be approximated by:

$$\mathbf{r}_\sigma = \sum_{h=1}^{M} N_h \mathbf{r}_h \text{ and } q = \sum_{h=1}^{M} N_h q_h; \quad (17)$$

where N_h is the known shape function; $\mathbf{r}_h$ is the local coordinate; q_h is the nodal values of the source strength; and M is the number of element nodes.

The discretized form of Eq. (16) based on the isoparametric transformation is given as:

$$p(\mathbf{r}) = \mathrm{i}\rho\omega\delta_\tau \sum_{i=1}^{K} \sum_{h=1}^{M} H_{ih}(\mathbf{r}) q_h; \quad (18)$$

where K is the number of elements and H_{ih} is given as:

$$H_{ih}(\mathbf{r}) = \int\limits_{\sigma_i} g(\mathbf{r}, \mathbf{r}_\sigma) N_h \mathrm{d}\sigma(\mathbf{r}_\sigma). \quad (19)$$

Equation (19) represented in the $s-t$ coordinate, for quadrilateral element and triangular element respectively, are the form of:

$$H_{ih}(\mathbf{r}) = \int_{-1}^{1}\int_{-1}^{1} g(\mathbf{r}, \mathbf{r}_\sigma(s,t)) N_h(s,t) J(s,t) \mathrm{d}s\mathrm{d}t; \quad (20)$$

$$H_{ih}(\mathbf{r}) = \int_{-1}^{1}\int_{-1}^{1-\eta} g(\mathbf{r}, \mathbf{r}_\sigma(s,t)) N_h(s,t) J(s,t) \mathrm{d}s\mathrm{d}t; \quad (21)$$

where $J(s,t)$ is the Jacobian of the transformation. For two-dimensional Gaussian quadrature formula, the upper bound of error is given as[20]:

$$\left| \int_{-1}^{1}\int_{-1}^{1} H(s,t) \mathrm{d}s\mathrm{d}t - \sum_{l=1}^{m}\sum_{j=1}^{n} w_l w_j H(s_l, t_j) \right| \le 2(E_1 + E_2); \quad (22)$$

where m and n denote the number of Gauss integral points in s and v direction, respectively; w_l and w_j are the Gauss weighting factor for the corresponding Gauss points s_l and s_j; E_1 and E_2 are the estimated relative errors.

The primary variations of the integrands in Eq. (20) and Eq. (21) are determined by the terms that can be characterized by $e^{-\mathrm{i}kr}/r^p,\ p = 1$ or 2. Therefore, the following integral can be representative of the actual integrals to estimate the Gaussian quadrature error bounds.

$$H = \int\limits_{\sigma_i} \frac{\mathrm{e}^{-\mathrm{i}kr}}{r^p} \mathrm{d}\sigma, \quad p = 1, 2, 3. \quad (23)$$

Table 1. The numbers of elements on the boundary for modes A and B.

	Mode A	Mode B
Sphere	82 TE	82 TE
Designed	774 TE+400QE	1686 TE

Considering that the Jacobian is almost constant within an element and the distance from the field point to the element is not severely varied, E_1 and E_2 are determined as[20]:

$$E_1 = \frac{\pi}{2(p-1)!}\left(\frac{kL_1}{4}\right)^{2m}\sum_{l=0}^{2m}\frac{(l+p-1)!}{l!(2m-l)!}\left(\frac{1}{kr_{\min}}\right); \tag{24}$$

$$E_2 = \frac{\pi}{2(p-1)!}\left(\frac{kL_2}{4}\right)^{2n}\sum_{l=0}^{2n}\frac{(l+p-1)!}{l!(2m-l)!}\left(\frac{1}{kr_{\min}}\right); \tag{25}$$

where $L_1 = \max(L_{12}, L_{34})$ and $L_2 = \max(L_{23}, L_{41})$; $r_{\min}$ is the minimum distance between the field point on the boundary and the element. To ensure convergence of the Gaussian quadrature, $k < \min(4/L_1, 4/L_2)$. For triangular element, the same criteria can be obtained. Let $L_{\max}$ denote the maximal size of all the elements on the optimal auxiliary surface. To make the prediction accuracy of acoustic pressure acceptable, the criterion should be satisfied.

$$k < 4/L_{\max}. \tag{26}$$

4. NUMEICAL SIMULATION

4.1. Validation of Equivalent Source Location Determination Method

In what follows, acoustic radiations from a uniformly pulsating sphere with radius $a = 1$ m and vibration velocity amplitude $v = 1$ m/s, and a radiator, as shown in Fig. 2, are presented to illustrate the use of the method. The acoustic medium is air with its density $\rho = 1.21$ kg/m^3, and the speed of acoustic $c = 343$ m/s. For the two radiators, the numbers of elements on the boundary for modes A and B are shown in Table 1, where TE and QE represent triangular and quadrilateral elements, respectively. Although there is no known analytical acoustic pressure for the designed radiator, an exact solution can be obtained using the substitute velocity boundaries, which is equivalent to that from a point source, that is, a simulation point source, in the structure surface. The prescribed normal velocity on the boundary surface is generated by placing an acoustic point source in the radiator. If the radiator vibrates under such a boundary condition, the radiated pressure must be equal to that generated by the point source. A monopole source that is a simulation point source is set at a fixed location with coordinate (0.15 m, 0 m, 0 m) for the designed radiator.

In this paper, $\varepsilon_1(\%)$ and $\varepsilon_2(\%)$ is used to represent the relative errors of the real and imaginary components of the predicted acoustic pressure, respectively. The root-mean square norms of them are given by:

$$\varepsilon_{\text{real}} = \sqrt{\frac{1}{M}\sum_{m=1}^{M}\varepsilon_{1m}^2}, \quad \varepsilon_{\text{imag}} = \sqrt{\frac{1}{M}\sum_{m=1}^{M}\varepsilon_{2m}^2}; \tag{27}$$

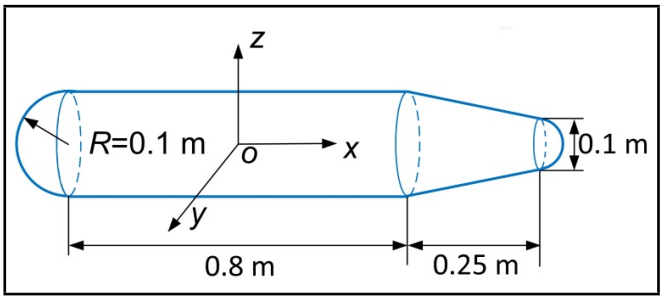

Figure 2. Shape and size of the designed radiator.

where ε_{1m} and ε_{2m} represent the relative errors of the real and imaginary components of the acoustic pressure at node $\mathbf{x}_m$, respectively. To study the effect of the equivalent source locations on the accuracy of the predicted result, ε_v, $\varepsilon_{\text{real}}$ and $\varepsilon_{\text{imag}}$ on boundary nodes of the two radiators are plotted for different k and S_c values in Figs. 3 and 4.

These results show that the locations have a remarkable influence on the accuracy of the predicted acoustic pressure, and that the errors change with S_c. Clearly, it can be seen that ε_v, $\varepsilon_{\text{real}}$ and $\varepsilon_{\text{imag}}$ show the almost identical trend, the prediction accuracy increases when ε_v decreases, and good prediction accuracy is obtained in the optimal auxiliary surface corresponding to minimum ε_v. Hence, ε_v is a good indicator of the prediction accuracy of the acoustic pressure. It is also observed that the prediction accuracy is relatively more sensitive to the source locations for complex radiator. From the data of the errors, the accuracy of the predicted values is acceptable at $0.19 \le S_c \le 0.37$ for the designed radiator.

To further test the effectiveness of the proposed method, the predicted acoustic pressure in optimal auxiliary surface is compared to those in other retracted surfaces on an arbitrary selected field point, $P_1 = (0$ m, 0 m, 1 m) and $P_2 = (0.15$ m, 0 m, 0.5 m) for the sphere and designed radiator, respectively. Figures 5 and 6 show the comparison results, where the calculation frequency k satisfies the requirement of $k \le 4/L_{\max}$.

The comparison results show that the numerical solutions in the optimal auxiliary surface are consistent with the exact solutions, and the prediction accuracy is significantly improved in the optimal auxiliary surface. Furthermore, it is shown again that the prediction accuracy is relatively more sensitive to the locations for complex radiator. According to analysis, the maximum errors of the predicted results are $1.4 \times 10^{-8}\%$ and $5.6 \times 10^{-3}\%$ for the sphere and designed radiator, respectively. However, in other retracted auxiliary surfaces, the prediction accuracy is very poor and the predicted result is unacceptable. Therefore, the optimal auxiliary surface must be determined.

4.2. Validation of Frequency Threshold Criterion

As previously analyzed, for a certain number of equivalent sources, the prediction accuracy is only good in a certain frequency range. Hence, it is necessary to judge the frequency range in which the prediction accuracy is acceptable. Figure 7 shows the plots of $\varepsilon_{\text{real}}$ and $\varepsilon_{\text{imag}}$ on boundary field nodes calculated in optimal auxiliary surfaces for different k. Obvi-

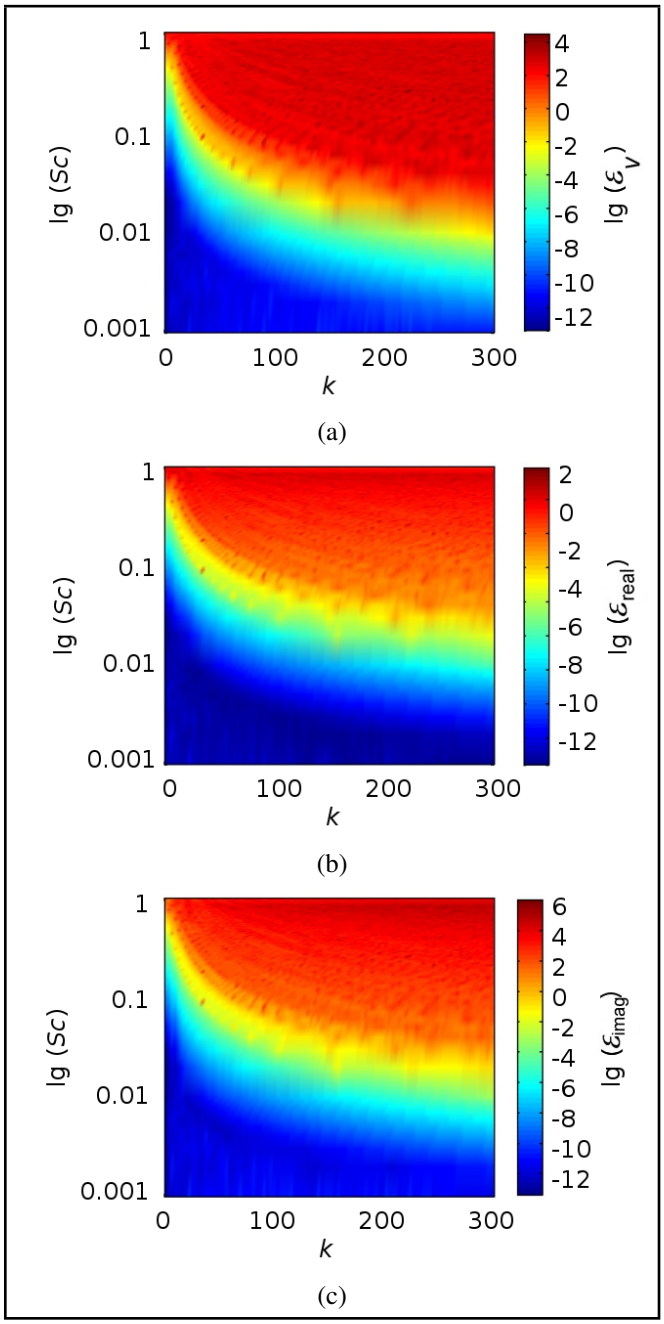

Figure 3. Plots of ε_v, $\varepsilon_{\text{real}}$ and $\varepsilon_{\text{imag}}$ on boundary nodes of uniformly pulsating sphere for different k and S_c values.

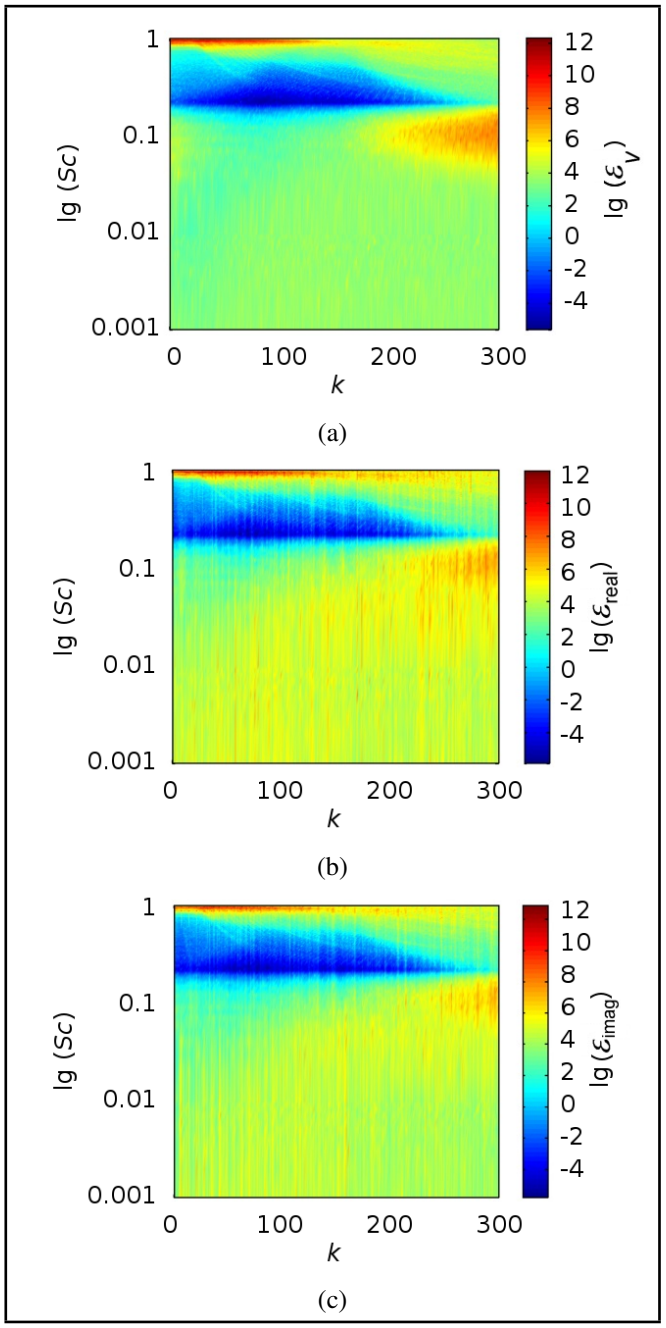

Figure 4. Plots of ε_v, $\varepsilon_{\text{real}}$ and $\varepsilon_{\text{imag}}$ boundary nodes of designed radiator for different k and S_c values.

Table 2. $k_{\text{threshold}}$ and maxima of $\varepsilon_{\text{real}}$ and $\varepsilon_{\text{imag}}$ on boundary field points calculated in optimal auxiliary surfaces when $k < k_{\text{threshold}}$.

	$k_{\text{threshold}}$	$\varepsilon_{\text{real}}$	$\varepsilon_{\text{imag}}$
Sphere	900	2.2×10^{-3}	1.00
Designed	270	0.70	1.05

ously, the accuracy of the predicted acoustic pressure becomes unacceptable when the acoustic wavenumber k exceeds a certain value. Table 2 shows the frequency $k_{\text{threshold}}$ that satisfies $k_{\text{threshold}} = 4/L_{\max}$ and the maxima of $\varepsilon_{\text{real}}$ and $\varepsilon_{\text{imag}}$ when $k < k_{\text{threshold}}$. The results show that the prediction accuracy is guaranteed by requiring $k < k_{\text{threshold}}$.

5. EXPERIMENTAL INVESTIGATION

To further validate the proposed method, the sound radiation of two radiators, namely, a cylindrical shell and a clamped plate are investigated experimentally, the physical data of which are shown in Table 3. The cylindrical shell with flanges of 1.5 cm thickness welded at its both ends is fixed on a still frame by bolt to approximate the clamped boundary condition, as shown in Fig. 8a. Both ends of the cylindrical shell are sealed by two aluminum alloy end plates with a thickness of 2 cm. This material is chosen because of its high stiffness and low weight. An ordinary 10 inch loudspeaker is positioned on an end plate to generate an interior sound field, which excites the cylindrical shell, as shown in Fig. 8c. The resulting structural vibration causes an exterior sound field around the cylin-

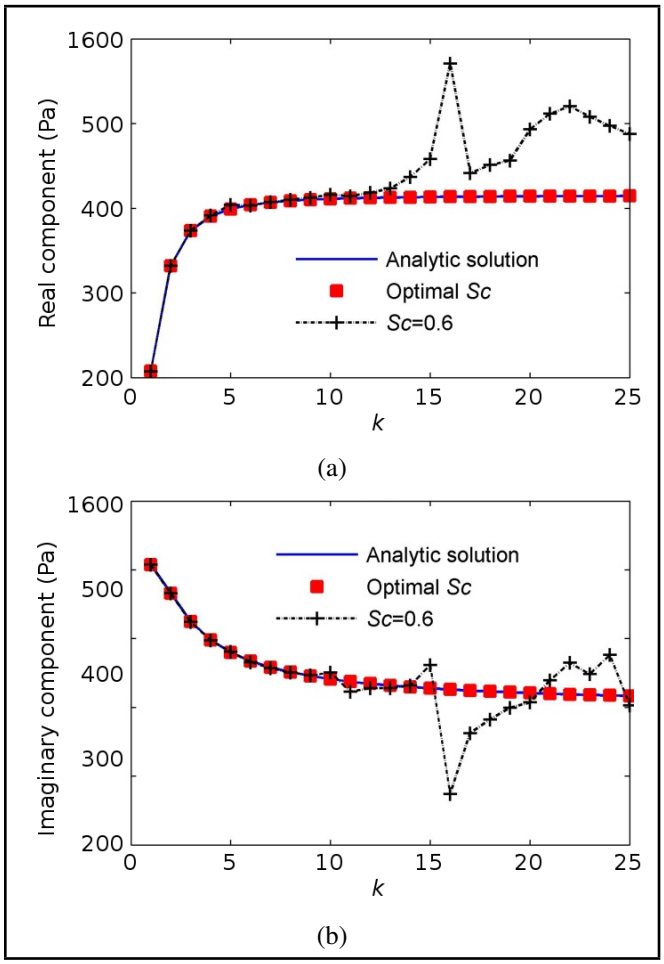

Figure 5. Variation of pressure in the selected field point with k for uniformly pulsating sphere.

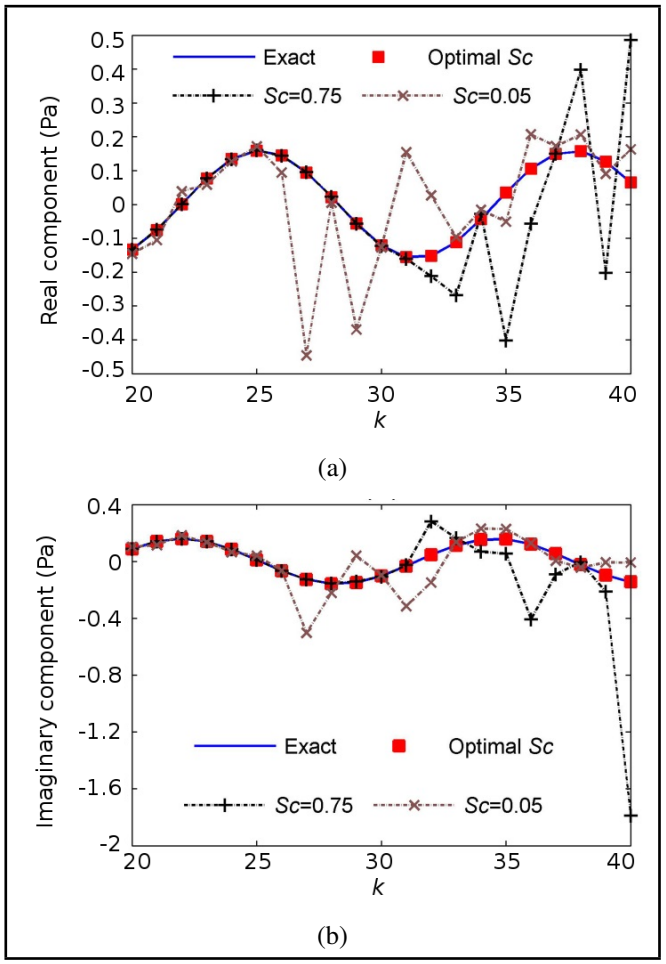

Figure 6. Variation of pressure in the selected field point with k for designed radiator.

Table 3. Physical data of two radiators.

	Cylindrical shell	Clamped plate
Length (m)	0.60	0.50
External diameter (m)	0.35	
Width (m)		0.50
Thickness (mm)	1.05.2018	1.08.2018
Density (kg/m^3)	7900	7800
Young' modulus (N/m)	1.95×10^{11}	2.1×10^{11}
Poisson Ratio	0.247	0.30
Loss factor	$10^{-4} \sim 10^{-3}$	$10^{-5} \sim 10^{-3}$

drical shell. The stiff plate is fixed with his rim on a stiff frame, the bottom of which holds an exciter, using bolt to approximate the clamped boundary condition, as shown in Fig. 8b. The exciter is connected to the center of the plate via a stiff push rod, as shown in Fig. 8d, and makes the plate vibrate to generate an exterior sound field.

The surfaces of the cylindrical shell and the clamped plate are divided evenly into 30 and 25 elements, respectively. The nodes of elements are used to obtain equivalent sources, and the normal velocities on the nodes are used to calculate the source strengths and the sound pressure. The constructed velocities $\hat{v}(\mathbf{r}_{sj})$ on the centers of the elements are interpolated using the measured velocities on the nodes. ε_v is obtained by substituting $\hat{v}(\mathbf{r}_{sj})$ and the measured velocities $v(\mathbf{r}_{sj})$ on the centers into Eq. (14). The normal velocities and the radiated acoustic pressure in the selected field points as depicted in Fig. 9 are obtained by means of velocity and pressure measurements, as shown in Fig. 10. For the cylindrical shell, the auxiliary surface is retracted from the boundary of the shell along x-axis, as shown in Fig. 9a. Considering that the stiff frame is well sealed, only the exterior side of the clamped plate generates sound field into the infinite domain. Thus, the auxiliary surface can be located on an auxiliary plane at a certain distance from the exterior side, as shown in Fig. 9b.

The measurements are made from 100 Hz to 700 Hz for the cylindrical shell and 100 Hz to 500 Hz for the clamped plate with increment of 10 Hz, the lower limit being imposed by the semi-anechoic laboratory. The loudspeaker and the exciter are driven with sinusoidal signal. The initial values of input volt age and current for the loudspeaker are 15 V and 1.6 A, and for the exciter 1.5 V and 2.7 A, where both the input voltages remain constant when the frequency is increased. The mass ratio of the used accelerometer to the cylindrical shell and clamped plate is less than 1%. Thus, the accelerometer has little influence on the vibration of the radiator. The measured and computed sound pressure levels are plotted in Figs. 11 and 12 for two radiators, where p_{amp} represents the amplitude of the acoustic pressure.

The results show that the prediction accuracy is significantly improved in the optimal auxiliary surface compared with the fixed auxiliary surface, and the computed pressures in the op-

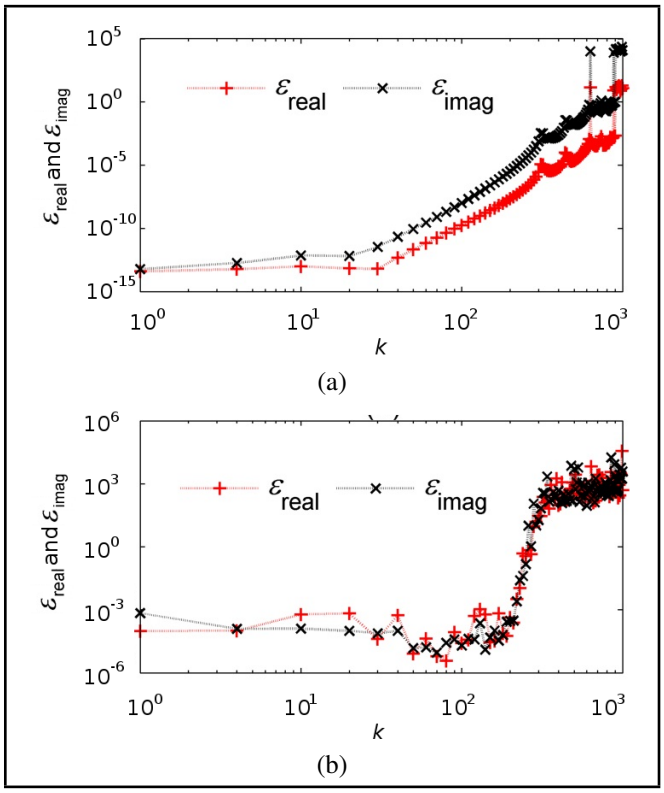

Figure 7. ε_{real} and ε_{imag} on boundary field points calculated in optimal auxiliary surfaces for different k (a) Uniformly pulsating sphere (b) Designed radiator.

Table 4. Prediction error in optimal auxiliary surface.

	Field point 1		Field point 2	
Relative errors %	Maximum	Average	Maximum	Average
Cylindrical shell	5.09	3.04	6.05	3.07
Clamped plate	13.05	8.02	21.09	10.04

timal auxiliary surfaces are consistent with the measured values. The detailed data of the calculation accuracy are shown in Table 4. From the data of the relative errors, the average and maximum errors corresponding to the cylindrical shell are less than 3.7% and 6.5%, respectively. The accuracy of the computed acoustic pressure is good. For the clamped plate, all of the accelerometer bases have been bonded to the surface of the clamped plate when the vibration velocity and acoustic pressure are measured. Its surface shape is changed by these bases. When the radiated pressure is computed, the surface is still treated as a plane. Its surface area is smaller than that of the cylindrical shell. Thus, the accuracy is lower than that corresponding to the shell. The average error is still acceptable, although the accuracies in very few frequencies are poor. In addition, there is still some reflection of sound wave. These cause discrepancy between the computed and measured values in several frequencies.

6. CONCLUSIONS

The selection of the auxiliary surface is the key to obtain accurate prediction results in the wave superposition method. The relationship between the surface velocity reconstruction error and acoustic pressure prediction error has been theoretically derived in this paper. Representative numerical examples show that the normalized velocity reconstruction error is a good indicator of the prediction error of acoustic pressure. The prediction accuracy can be significantly improved in the optimal auxiliary surface compared with the fixed auxiliary surface. With the criterion satisfied, the prediction accuracy in the optimal auxiliary surface is acceptable and significantly improved. The experimental results show that the prediction error of acoustic pressure in the determined optimal auxiliary surface is greatly reduced. Thus, the proposed method is good at reducing the prediction error and is feasible.

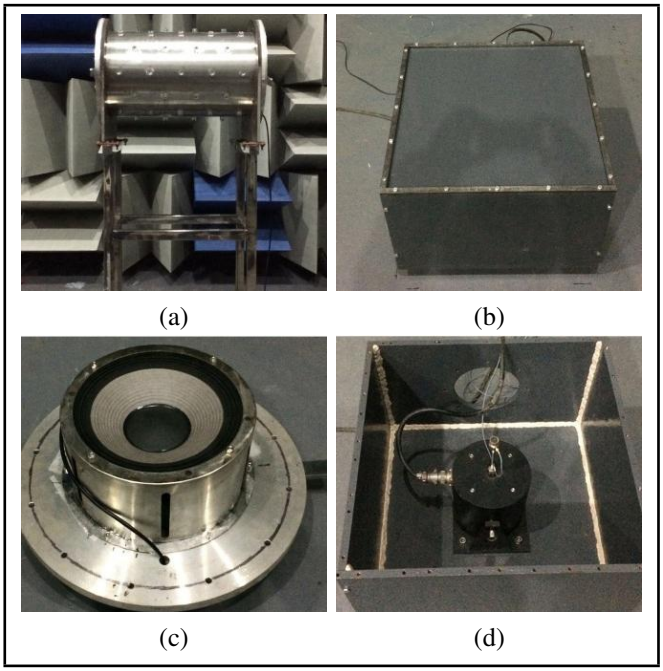

Figure 8. (a) Steel cylindrical shell (b) Clamped plate(c) Loudspeaker (d) Exciter.

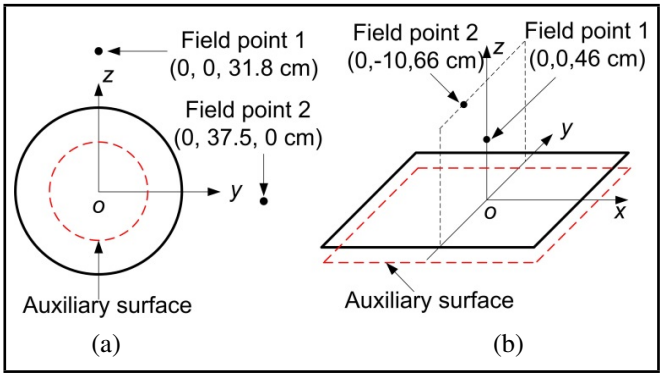

Figure 9. Coordinates of these field points (a) Cylindrical shell (b) Clamped plate.

ACKNOWLEDGEMENTS

This work was supported by the National Natural Science Foundation of China (“Research on structure sound radiation matrix deriving, computing and optimizing”, Grant No.51079118; “Research on computational auditory scene analysis based internal combustion engine noise sources identification”, Grant No.51279148).

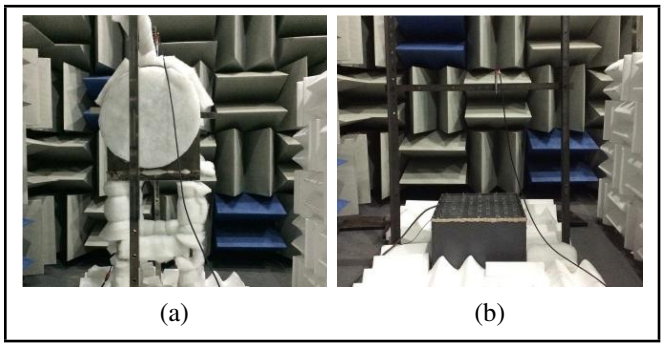

Figure 10. Acoustic pressure measurement (a) Cylindrical shell (b) Clamped plate.

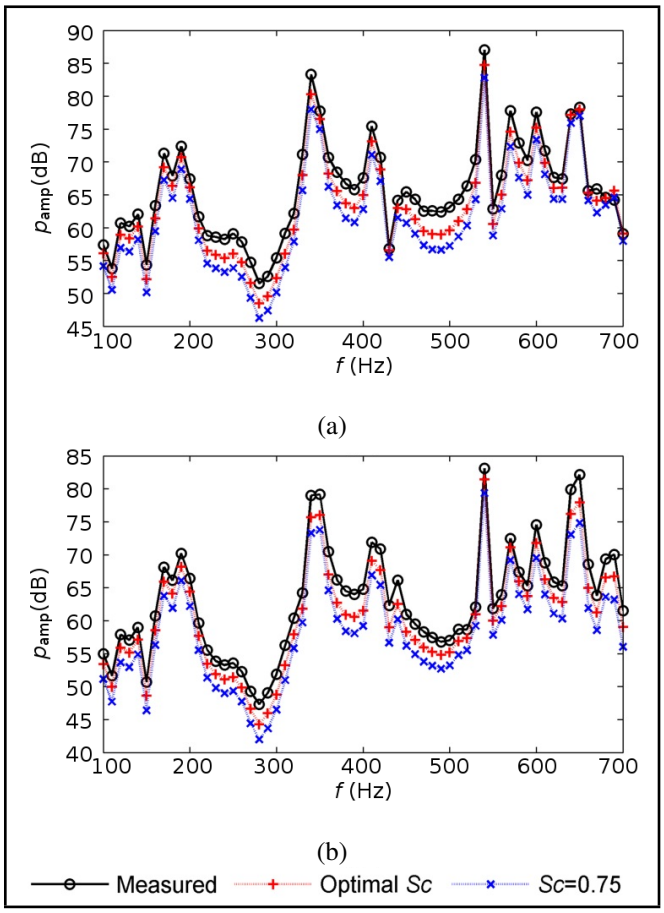

Figure 11. Amplitude of the acoustic pressure of the cylindrical shell at the selected field points (a) Field point 1 (b) Field point 2.

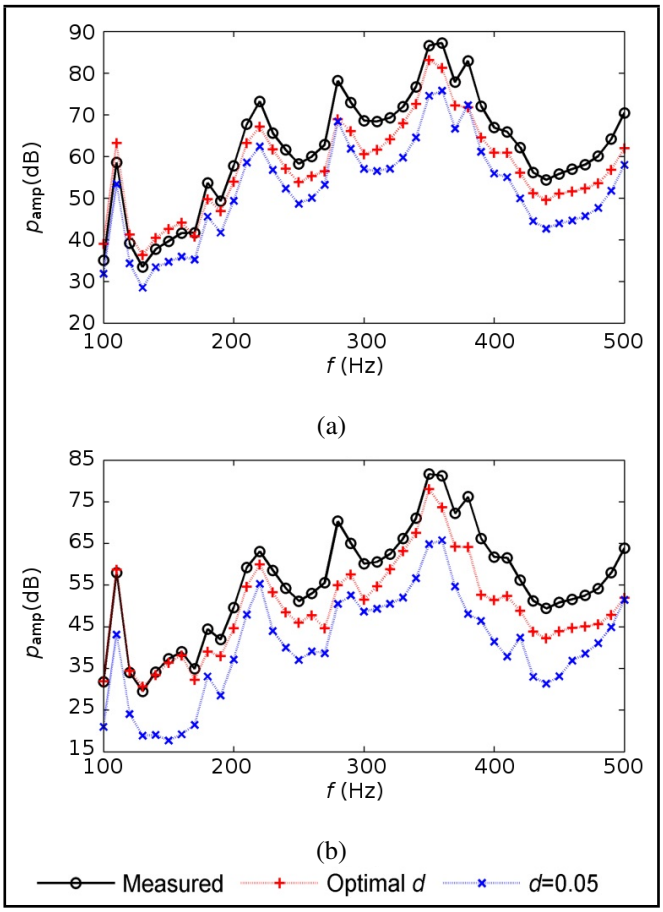

Figure 12. Amplitude of the acoustic pressure of the clamped plate at the selected field points (a) Field point 1 (b) Field point 2.

REFERENCES

[1] Harari, I. and Hughes, T. J. R. Galerkin/least-squares finite element methods for the reduced wave equation with non-reflecting boundary conditions in unbounded domains, *Comput. Methods Appl. Mech. Eng.*, **98** (3), 411–454, (1992). https://dx.doi.org/10.1016/0045-7825(92)90006-6

[2] Harari, I. and Hughes, T. J. R. A cost comparison of boundary element and finite element methods for problems of time-harmonic acoustics, *Comput. Methods Appl. Mech. Eng.*, **97** (1), 77–102, (1992). https://dx.doi.org/10.1016/0045-7825(92)90108-V

[3] Thompson, L. L. A review of finite-element methods for time-harmonic acoustics, *J. Acoust. Soc. Am.*, **119** (3), 1315–1330, (2006). https://dx.doi.org/10.1121/1.2164987

[4] Visser, R. *A boundary element approach to acoustic radiation and source identification*, PhD Thesis, University of Twente, The Netherlands, (2004).

[5] Gong, J. Y., An, J. Y., Ma, L., and Xu, H. T. Numerical quadrature for singular and near-singular integrals of boundary element method and its applications in large-scale acoustic problems, *Acta Ac.*, **41** (5), 768–775, (2016). https://dx.doi.org/10.15949/j.cnki.0371-0025.2016.05.029

[6] Zheng, L., Zhang, D., Liu, C., and Li, Y. Topology optimization of a constrained layer damping plate coupled with an acoustical cavity, *Int. J. Acoust. Vib.*, **21** (4), 394–405, (2016). https://dx.doi.org/10.20855/ijav.2016.21.4434

[7] Mosiamisi, M. Implementation of a boundary element method for high frequency scattering by convex polygons with impedance boundary conditions, *Int. J. Acoust. Vib.*, **21** (4), 470–477, (2016). https://dx.doi.org/10.20855/ijav.2016.21.4442

[8] Liu, X., Wu, H., and Jiang, W. Hybrid approximation hierarchical boundary element methods for acoustic problems, *J. Comput. Acoust.*, **25** (3), 1750013, (2017). https://dx.doi.org/10.1142/S0218396X17500138

[9] Cutanda Henrìquez, V., Andersen, P. R., Jensen, J. S., Juhl, P. M., and Sànchez-Dehesa, J. A Numerical Model of an Acoustic Metamaterial Using the Boundary Element Method Including Viscous and Thermal Losses, *J. Comput. Acoust.*, **25** (4), 1750006, (2016). https://dx.doi.org/10.1142/S0218396X17500060

[10] Koopmann, G. H., Song, L., and Fahnline, J. B. A method for computing acoustic fields based on the principle of wave superposition, *J. Acoust. Soc. Am.*, **86** (6), 2433–2438, (1989). https://dx.doi.org/10.1121/1.398450

[11] Davey, K. and Farooq, A. Evaluation of free terms in hypersingular boundary integral equations, *Eng. Anal. Bound. Elem.*, **35** (9), 1060–1074, (2011). https://dx.doi.org/10.1016/j.enganabound.2011.04.002

[12] D'Amico, R., Neher, J., Wender, B., and Pierini, M. On the improvement of the solution accuracy for exterior acoustic problems with BEM and FMBEM, *Eng. Anal. Bound. Elem.*, **36** (7), 1104–1115, (2012). https://dx.doi.org/10.1016/j.enganabound.2012.02.009

[13] Steffen, M. Numerical damping in the acoustic boundary element method, *Acta Acust. United Ac.*, **102** (3), 415–418, (2016). https://dx.doi.org/10.3813/AAA.918958

[14] Lock, A. and Holloway, D. Boundary element modelling of a novel simple enhanced bandwidth schroeder diffuser offering comparable performance to a fractal design, *Acoust. Aust.*, **44** (1), 137–147, (2016). https://dx.doi.org/10.1007/s40857-016-0049-4

[15] Hwang, Y. S. *A wave superpostion method formulation in digital acousitc space*, PhD Thesis, Pennsylvania State University, USA, (2009).

[16] Bai, M. R., Hsu, H., and Wen, J. C. Spatial sound field synthesis and upmixing based on the equivalent source method, *J. Acoust. Soc. Am.*, **135** (1), 269–282, (2014). https://dx.doi.org/10.1121/1.4835815

[17] Rafael, P., Haike, B., and Martin, O. et al. Equivalent source method and boundary element method for calculating combustion noise, *Acta Acust. United Ac.*, **94** (4), 514–527, (2008). https://dx.doi.org/10.3813/AAA.918060

[18] Bai, M. R. and Chen, C. C. On optimal retreat distance for the equivalent source method-based near field acoustical holography, *J. Acoust. Soc. Am.*, **129** (3), 1407–1416, (2011). https://dx.doi.org/10.1121/1.3533734

[19] Fahnline J. B. and Koopmann, G. H. A numerical solution for the general radiation problem based on the combined methods of superposition and singular-value decomposition, *J. Acoust. Soc. Am.*, **90** (90), 2808–2819, (1991). https://dx.doi.org/10.1121/1.401878

[20] Hwang, Jyh-Y. and Chang, S. C. A retracted boundary integral equation for exterior acoustic problem with unique solution for all wave numbers, *J. Acoust. Soc. Am.*, **90** (2), 1167–1180, (1990). https://dx.doi.org/10.1121/1.402022

[21] Gounot, Y. J. R. and Musafir, R. E. On appropriate equivalent monopole sets for rigid body scattering problems, *J. Acoust. Soc. Am.*, **122** (6), 3195–3205, (2007). https://dx.doi.org/10.1121/1.2799504

[22] Gounot, Y. J. R. and Musafir, R. E. Genetic algorithms: a global search tool to find optimal equivalent source sets, *J. Sound Vib.*, **322** (1–2), 282–298, (2009). https://dx.doi.org/10.1016/j.jsv.2008.11.001

[23] Gounot, Y. J. R. and Musafir, R. E. Simulation of scattered fields: Some guidelines for the equivalent source method, *J. Sound Vib.*, **330** (15), 3698–3709, (2009). https://dx.doi.org/10.1016/j.jsv.2011.03.006

[24] Zellers, B. C. *An Acoustic Superposition Method For Computing Structural Radiation In Spatially Digitized Domains*, PhD Thesis, Pennsylvania State University, USA, (2006).

[25] Zellers, B. C., Koopmann, G. H., and Jonson, M. L. An Acoustic Superposition Method for Computing Structural Radiation in Spatially Digitized Domains, Proc. *2007 ASME International Mechanical Engineering Congress and Exposition*, Washington, USA, (2007). https://dx.doi.org/10.1115/IMECE2007-41313

[26] Wu, S., Xiang, Y., Xia, X., and Wang, X. Research on a method for acoustic superposition in element free spatial discrete domains, *J. Huazhong Univ. Sci. & Tech. (Natural Science Edition)*, **41** (11), 22–25, (2014). https://dx.doi.org/10.13245/j.hust.2013.11.002

[27] Wu, S., Xiang, Y., and Xia, X. Approximate analytical expressions of self-radiation terms including acoustic pressure and velocity based on element free acoustic wave superposition, *J. Vib. Shock*, **33**(7), 79–85, (2014). https://dx.doi.org/10.13465/j.cnki.jvs.2014.07.014

[28] Koopmann, G. H. *Designing quiet structures*, Academic Press, California, USA, (1997).